

Discovery of a young and massive stellar cluster

Spectrophotometric near-infrared study of Masgomas-1

S. Ramírez Alegría^{1,2}, A. Marín-Franch^{3,4}, and A. Herrero^{1,2}

¹ Instituto de Astrofísica de Canarias, 38205 La Laguna, Tenerife, Spain
e-mail: sramirez@iac.es

² Departamento de Astrofísica, Universidad de La Laguna, 38205 La Laguna, Tenerife, Spain

³ Centro de Estudios de Física del Cosmos de Aragón (CEFCA), 44001 Teruel, Spain
e-mail: amarin@cefca.es

⁴ Departamento de Astrofísica, Universidad Complutense de Madrid, 38040 Madrid, Spain

Received 14 October 2011 / Accepted 13 March 2012

ABSTRACT

Context. Recent near-infrared data have contributed to the discovery of new (obscured) massive stellar clusters and massive stellar populations in previously known clusters in our Galaxy. These discoveries lead us to view the Milky Way as an active star-forming machine.

Aims. The main purpose of this work is to determine physically the main parameters (distance, size, total mass and age) of Masgomas-1, the first massive cluster discovered by our systematic search programme.

Methods. Using near-infrared (J , H , and K_S) photometry we selected 23 OB-type and five red supergiant candidates for multi-object H - and K -spectroscopy and spectral classification.

Results. Of the 28 spectroscopically observed stars, 17 were classified as OB-type, four as supergiants, one as an A-type dwarf star, and six as late-type giant stars. The presence of a supergiant population implies a massive nature of Masgomas-1, supported by our estimate of the cluster initial total mass of $(1.94 \pm 0.28) \times 10^4 M_\odot$, obtained after integrating the cluster mass function. The distance estimate of $3.53^{+1.55}_{-1.40}$ kpc locates the cluster closer than the Scutum-Centaurus base but still within that Galactic arm. The presence of an O9 V star and red supergiants in the same population indicates that the cluster age is in the range of 8 to 10 Myr.

Key words. infrared: stars – supergiants – stars: early-type – techniques: spectroscopic – techniques: photometric – stars: massive

1. Introduction

Massive stars are key components in the Galactic evolution. They change the star formation rate, ionize their surrounding media with their winds, strengthen the formation of other stars, or deplete their native clouds through their own birth. They are short-lived objects, and their impact on the interstellar medium also occurs on short times scales, playing a crucial role in the energy balance, dynamics, and chemical evolution of their host galaxy. We often find them embedded in obscured massive clusters characterized by high-extinction regions. Unfortunately, owing to this strong extinction, the optical detection of these objects is difficult, but they can be detected and observed using near-infrared instrumentation. All-sky surveys such as 2MASS (Skrutskie et al. 2006), GLIMPSE (Benjamin et al. 2003), and UKIDSS (Lawrence et al. 2007) have allowed the discovery of the most massive stellar clusters in the Galaxy. Nevertheless, the census of massive clusters is far from complete; up to 100 clusters with a mass greater than $10^4 M_\odot$ may remain hidden (Hanson & Popescu 2008). Systematic search programmes for these objects are necessary for a full understanding of our Galaxy.

The MASGOMAS project (Marín-Franch et al. 2009) has recently started a systematic search for massive cluster candidates in the Galactic disc. In a quick exploration using our search

algorithm we have found a new massive cluster candidate, located near the direction of the Scutum-Centaurus arm base, and previously unidentified in the literature.

In this exciting region, where the Scutum-Centaurus arm meets the Galactic central bar, several red supergiant clusters have been found: RSGC 1 (Figer et al. 2006; Davies et al. 2008), RSGC 2 (Davies et al. 2007), RSGC 3 (Clark et al. 2009a), and CI Alicante 8 (Negueruela et al. 2010). These massive clusters (each of them having a total mass estimate greater than $10^4 M_\odot$) are remarkable because of their population of red supergiant (RSG) stars, ranging between 8 and 26 RSGs. Their presence within a concentrated area in the Galactic plane ($l = 24^\circ - 29^\circ$) and a similar distance ($d \sim 6$ kpc), makes this region extremely interesting for searching massive cluster candidates.

The first new massive cluster candidate discovered by our group, and labelled as Masgomas-1, is located in the Galactic plane near the Scutum-Centaurus base ($l = 33^\circ 11' 12''$, $b = +0^\circ 42'$, and $\alpha_{2000} = 18^{\text{h}} 50^{\text{m}} 15^{\text{s}}$, $\delta_{2000} = +00^\circ 21' 04''$). Masgomas-1 lies near the IRAS source IRAS 18497+0022, a very bright object in the *Spitzer* 8.0 μm image, which extends over $\sim 0.35^\circ$ (see Fig. 1). In the surroundings of Masgomas-1 we find two other IRAS sources (IRAS 18476+0017, IRAS 18476+0019), and the radio source GPSR 033.086+0.434. An inspection of 2MASS photometry of the smaller area within the square in Fig. 1 reveals the presence of three bright and red stars



Fig. 1. *Spitzer* 8.0 μm image section for the region around IRAS 18497+0022. The *Spitzer* section covers an area of 15×50 square arc minutes and includes Masgomas-1, shown as observed with LIRIS on the left side of the image. The length of the orientation arrows is 2.5 arcmin.

($K_S < 6$ and $J - K_S \sim 4$), separated by ~ 2 mag in K_S from the other field stars. This characteristic has been observed previously in the red supergiant population of RSGC 1, 2, 3, and Alicante 8, making these three Masgomas-1 stars red supergiant candidates.

In this article we describe our systematic search for massive stellar candidates based on the detection of OB-type star candidate over-densities (Sect. 2) and spectrophotometric observations of Masgomas-1 (Sect. 3). In Sect. 4 we describe the near-infrared photometry of the cluster, the spectral classifications of the 28 spectroscopically observed stars, and the proper motion measures for 20 of them. An analysis of the cluster physical parameters (distance, extension, mass, and age) is given in Sect. 5. Our main results are summarized in Sect. 6.

2. Systematic search of obscured clusters and candidate selection

For our preliminary cluster search we have used 2MASS photometry (Skrutskie et al. 2006), focused on Galactic coordinates in the ranges $l = 20^\circ - 45^\circ$ and $b = 0^\circ - 5^\circ$. This area was divided into smaller regions of 5×5 square degrees. Only stars with J -, H -, and K_S -bands and good data quality (defined by photometric errors less than 0.1 and quality flags equal to “AAA”) were used in the candidate search.

To select OB-type star candidates, we have filtered the photometry using the following criteria:

1. K_S magnitude less than 12: by defining this limiting magnitude we aimed to prevent Poisson noise, derived from the field stellar distribution, from prevailing over the candidate over-densities.
2. Red ($J - K_S$) colours: unreddened foreground disc stars exhibit bluer colours in the CMD. To eliminate most of these stars from our systematic search, we applied a cut in ($J - K_S$), discarding objects with $(J - K_S) < 0.5$.
3. Reddening-free parameter between -0.3 and 0.3 : the reddening-free parameter Q_{IR} , described by Comerón & Pasquali (2005) and Negueruela & Schurch (2007), has a value close to zero for OB stars. Considering photometric errors we define a range for Q_{IR} where OB-star candidates would be expected. However, because A- and early F-type stars can mimic the Q_{IR} of an OB star, contamination by these stellar types is plausible.

Using the sources that fulfil the previous criteria, which assures a selection of OB-star candidates, we looked for over-densities of these stars to identify them as massive cluster candidates. One of these cluster candidates, without previous identification in the literature, is Masgomas-1.

For Masgomas-1 most of the OB-type star candidates detected as an overdensity using the near-infrared data does not appear in optical images of the region. Even the central bright stars marked with red circles in Fig. 2 remains undetected in optical bands. The overdensity is concentrated within a ~ 1.5 radius and triplicates the number of OB-type candidates found in a control ring, which is concentric and covers same area as the central search area.

3. Observations of Masgomas-1

We based our study of Masgomas-1 on broad-band near-infrared imaging (J , H , K_S), medium resolution multi-object spectroscopy (H and K) and long-slit spectroscopy (H and K). All data were acquired with LIRIS, a near-infrared imager/spectrograph mounted at the Cassegrain focus of the 4.2 m *William Herschel* Telescope (WHT; Roque de Los Muchachos Observatory, La Palma). A summary of the observations is given in Table 1.

3.1. Imaging

The cluster candidate was observed on 2010 June 23 using LIRIS, an infrared camera equipped with a Hawaii 1024 \times 1024 HgCdTe array detector, with a field of view of $4.2' \times 4.2'$ and a spatial scale of $0''.25 \text{ pixel}^{-1}$. Images were obtained for filters J ($\lambda_C = 1.250 \mu\text{m}$, $\Delta\lambda = 0.160 \mu\text{m}$), H ($\lambda_C = 1.635 \mu\text{m}$, $\Delta\lambda = 0.290 \mu\text{m}$) and K_S ($\lambda_C = 2.150 \mu\text{m}$, $\Delta\lambda = 0.320 \mu\text{m}$), with seeing values between $0''.69$ and $0''.80$.

To improve cosmic-ray and bad-pixel rejection, and to construct the sky image for subtraction, we observed on a nine-point dithering mode. Data reduction (bad-pixel mask, flat correction, sky subtraction and alignment) was made with FATBOY (Eikenberry et al. 2006) and geometrical distortions were corrected with the LIRIS reduction package LIRISDR¹. The final K_S image for Masgomas-1 is shown in Fig. 2. In the K_S image, as well as for the J and H images, three bright stars stand out,

¹ <http://www.iac.es/project/LIRIS>

Table 1. Summary of imaging and spectroscopic observations.

Observation mode	Date	Filter	Exp. time [s]	Seeing [$''$]
Masgomas-1 field imaging	2010-06-23	<i>J</i>	108.0	0.80
	2010-06-23	<i>H</i>	36.0	0.76
	2010-06-23	<i>K_S</i>	36.0	0.69
Multi-object spectroscopy ($R \sim 2500$), mask A	2010-06-23	<i>H</i>	4800.0	0.76
	2010-06-24	<i>K</i>	4800.0	0.80
Multi-object spectroscopy ($R \sim 2500$), mask B	2010-06-25	<i>H</i>	1920.0	0.84
Long-slit spectroscopy ($R \sim 2500$)	2010-06-23	<i>H</i>	720.0	0.64
	2010-06-24	<i>H</i>	480.0	0.56
	2010-06-24	<i>K</i>	320.0	0.60
	2011-09-15	<i>H</i>	420.0	0.55
	2011-09-15	<i>K</i>	260.0	0.72

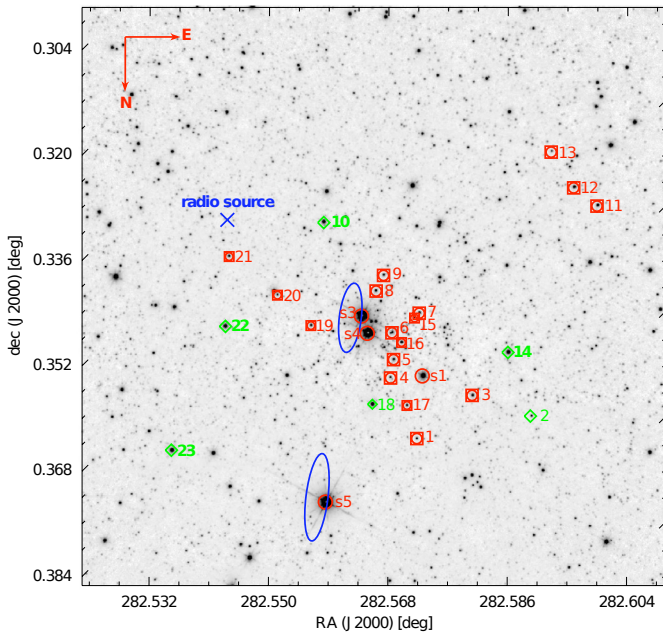


Fig. 2. LIRIS K_S image of Masgomas-1; the stars observed spectroscopically with the multi-object masks are shown with red squares (early-type stars), and green diamonds (A- and late-type disc stars). Bright stars observed with long-slit spectroscopy are marked with red circles. The position of star s02, observed with long-slit, is not shown in the figure because it lies 30 arcsec to the right of the field. Blue ellipses correspond to the 1σ positional uncertainties for the IRAS 18476+0017 (central) and IRAS 18476+0019 (lower) sources. The (blue) cross shows the position of the radio source GPSR 033.086+0.434.

two of them in the centre of the field (s03, s04 and s05). These two central bright stars, observed with long-slit spectroscopy as described in next section, set the centre of our cluster candidate. We also marked in the image the position of the spectroscopically observed OB-type candidates. Most of the candidates are concentrated around the aforementioned bright central stars, and the central coordinates of the OB-type candidates overdensity coincide with the position of the bright central stars.

Instrumental photometry was made with DAOPHOT II, ALLSTAR and ALLFRAME (Stetson 1994). The photometry was cleaned of non-stellar and poorly measured objects using ALLFRAME sharp index ($-0.25 < \text{sharp} < 0.25$) and PSF fitting σ (less than 0.1). The photometric calibration for the three filters was performed using sources from the 2MASS catalogue. We selected 362 isolated and non-saturated stars

with photometry in 2MASS, well distributed over the images and the $(J - K_S) - K_S$ colour–magnitude diagram. For stars with K_S less than 9 mag, we adopted the 2MASS photometry, due to saturation.

The astrometrical calibration was performed with SKYCAT, matching physical and equatorial coordinates for 14 sources that are well-distributed in our LIRIS image. Typical values for the fitting rms were less than 0.15 arcsec for the three bands, which was adequate for the mask design requirement.

3.2. Infrared spectroscopy

The near-infrared spectra were obtained on 2010 June 23–25, and 2011 September 15, using multi-object and long-slit spectroscopy observing modes.

For the multi-object spectroscopic (MOS) mode we designed two masks for OB-type stellar candidates. Mask A contained thirteen stars and mask B ten stars. The selection of stars considered a K_S dispersion less than 2 mag for the same mask to avoid large differences in the integration times and the spectral signal-to-noise ratios (S/Ns). We also selected stars with reddening-free parameter Q_{IR} between -0.3 and 0.3 (characteristic of OB-type stars) and K_S less than 12.5 mag.

The mask design also took into consideration the spectral range derived from the slit position. Slits located in the right half of the detector obtain spectra from 1.55 to 1.85 μm in the *H*-band and from 2.06 to 2.40 μm in the *K*-band. These spectral ranges include the He I 1.70 μm , He I 2.11 μm , He II 2.57 μm , and He II 1.69 μm lines, which are required for early-type stellar spectral identification and classification.

Objects for mask A were observed using the *H* and *K* pseudogrism, and those for mask B with the *H* pseudogrism. The spectral resolution of the pseudogrisms was $\lambda/\Delta\lambda \sim 2500$ and seeing values during observations, measured from the telluric lines in the spectra, were between 0.76 and 0.86 arcsec. Slits vary between 9 and 10 arcsec long and 0.85 arcsec wide.

For long-slit spectroscopy we selected five bright red supergiant candidates. Stars with similar magnitudes were paired to obtain spectra with similar S/Ns. The slit was 0.75 arcsec wide and, because we used the same pseudogrism as for the MOS observations, the resolution was also $\lambda/\Delta\lambda \sim 2500$.

We observed with an ABBA strategy (the star is located in positions A and B in the slit, the positions then being sequentially changed); with this mode, we were able to remove the sky from the spectra by subtracting spectra at position A from spectra at position B, and vice versa. Flat-fielding, spectral tracing, sky subtraction, coaddition, and extraction were applied using

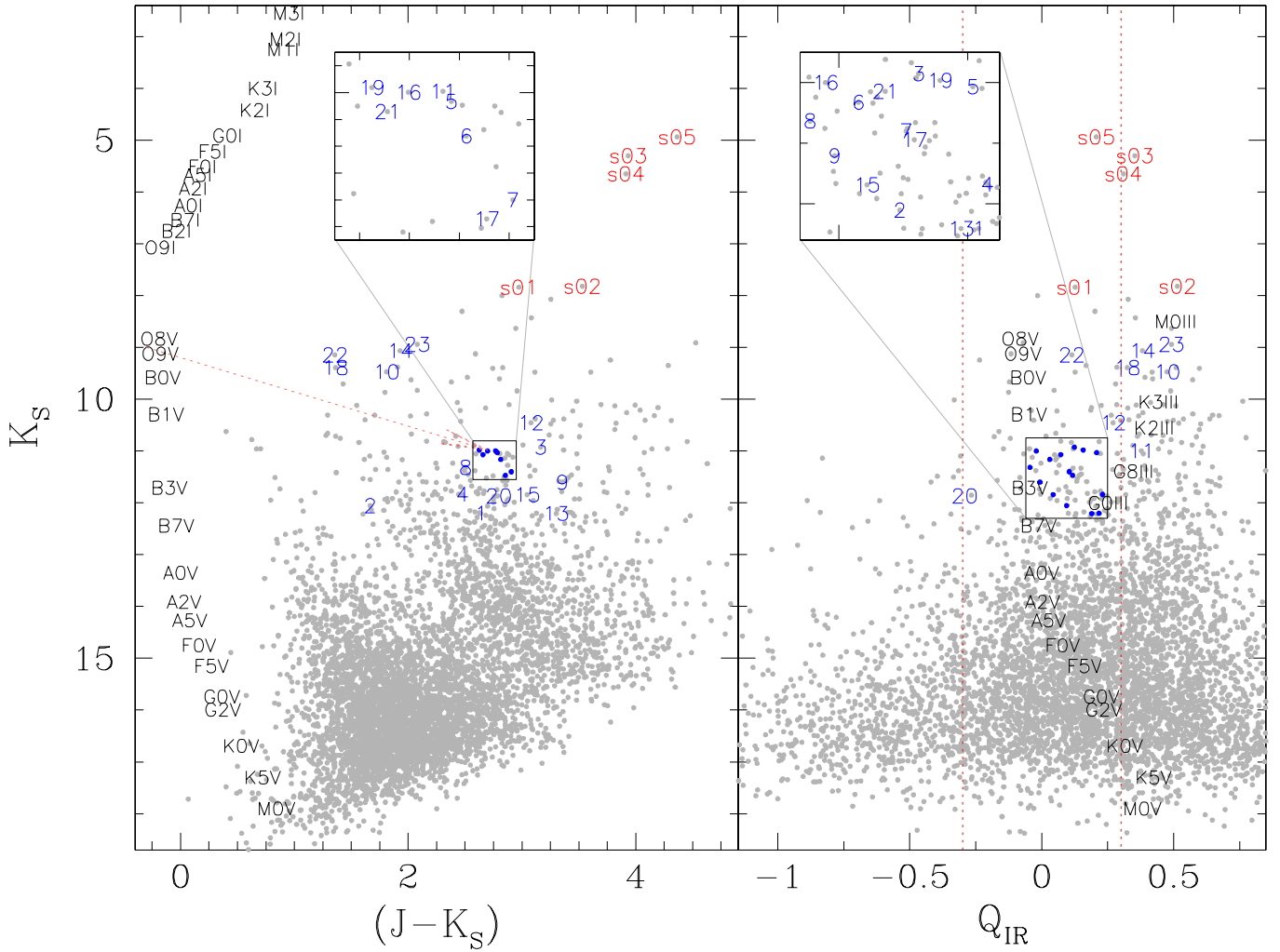


Fig. 3. Calibrated colour–magnitude (*left*) and free-reddening parameter–magnitude (*right*) diagrams for Masgomas-1. The red segmented arrow in *the left panel* shows $A_{K_S} = 3.00$. Main sequence and supergiant sequence, shown in black, are located without reddening at the distance determined in this study (3.53 kpc). In *the right panel* the red segmented lines show the limit for the Q_{IR} parameter used in the systematic search. The expected Q_{IR} and K_S magnitude for the dwarf and giant sequences located at the distance determined in this study (3.53 kpc) are also shown in black. In both diagrams the positions of the spectroscopically observed stars are marked with blue (multi-object spectroscopy) and red numbers (long-slit spectroscopy). We marked the stars located in the central regions of both diagrams with blue circles and amplified the regions in the upper squares, where the observed stars are marked with blue numbers. We used visual magnitudes and intrinsic colours from Cox (2000) for deriving the dwarf, giant, and supergiant sequences.

IRAF² for the long-slit spectra and LIRISDR, a package developed specifically for LIRIS data, which uses the information from the mask design files for the MOS spectra.

Combining the individual spectra, we discarded cosmic rays and hot pixels that might mimic spectral lines. For wavelength calibration, argon and xenon lamps were observed, both lamps (continuum-subtracted) being used to calibrate the K -band spectra and the argon lamp only for the H -band spectra.

Three A0V stars were observed as telluric standards: V 1431 Aql, HD 177724, and HD 167163. Telluric subtraction was carried out using XTELLCOR (Vacca et al. 2003), an IDL program that, applying a high-resolution synthetic model of an A0V star (the spectral type of our standard) over the observed telluric standards, produces the calibration spectrum with the

telluric lines. This spectrum was then used to correct our science spectra with the IRAF task TELLURIC.

4. Results

4.1. Colour–magnitude diagram

From the cluster’s CMD we selected the OB-type candidates, using the Q_{IR} selection method described in Sect. 2. The differential extinction seems to be high for Masgomas-1, as can be noted by the range of colour where the cluster candidate OB stars are distributed (see Fig. 3).

In the right panel of Fig. 3 the Q_{IR} parameter for dwarf and giant stars can be seen. Note that it is easy to separate both luminosity classes using the reddening-free parameter. In the same figure it is also noticeable that A- and early F-stars can mimic an OB star, as mentioned in Sect. 2; contamination by A- or F-type stars is expected in our set. Finally, we also find stars that satisfy the Q_{IR} requirement (e.g. stars with the numbers 2, 18, and 22),

² IRAF is distributed by the National Optical Astronomy Observatories, which are operated by the Association of Universities for Research in Astronomy, Inc., under cooperative agreement with the National Science Foundation.

Table 2. Spectroscopically observed stars.

ID	RA (J2000) [^h ^m ^s]	Dec (J2000) [[°] ['] ^{''}]	<i>J</i> [mag]	<i>H</i> [mag]	<i>K_S</i> [mag]	Spectral type	<i>A_{K_S}</i>	Distance [kpc]
Star cluster candidates:								
1	18 50 17.398	+00 22 04.77	14.843	13.101	12.204	B1 V	1.83 ^{+0.03} _{-0.02}	3.69 ^{+2.54} _{-1.75}
3	18 50 19.420	+00 21 41.15	14.089	12.051	10.925	O9 V	2.21 ^{+0.01} _{-0.03}	2.95 ^{+0.88} _{-1.20}
4	18 50 16.434	+00 21 31.44	14.316	12.671	11.839	B0 V	1.74 ^{+0.02} _{-0.03}	4.50 ^{+1.80} _{-2.14}
5	18 50 16.555	+00 21 21.69	13.817	11.987	11.033	O9.5 V	1.95 ^{+0.01} _{-0.03}	3.14 ^{+0.82} _{-1.08}
6	18 50 16.500	+00 21 07.01	13.976	12.193	11.162	B0 V	1.96 ^{+0.02} _{-0.03}	2.98 ^{+1.19} _{-1.42}
7	18 50 17.481	+00 20 56.26	14.307	12.438	11.400	O9.5 V	2.03 ^{+0.01} _{-0.03}	3.58 ^{+0.94} _{-1.23}
8	18 50 15.903	+00 20 44.31	13.821	12.261	11.317	O9.5–B0 V	1.76 ^{+0.02} _{-0.03}	3.70 ^{+1.21} _{-1.86}
9	18 50 16.185	+00 20 35.77	14.958	12.848	11.603	O9.5 V	2.33 ^{+0.01} _{-0.03}	3.43 ^{+0.90} _{-1.18}
11	18 50 23.945	+00 19 57.52	13.762	11.880	10.995	O9 V	1.95 ^{+0.01} _{-0.03}	3.43 ^{+1.02} _{-1.40}
12	18 50 23.091	+00 19 47.64	13.535	11.496	10.456	O9 V	2.15 ^{+0.01} _{-0.03}	2.44 ^{+0.73} _{-0.99}
13	18 50 22.271	+00 19 28.18	15.505	13.357	12.205	B0 V	2.29 ^{+0.02} _{-0.03}	4.15 ^{+1.66} _{-1.98}
15	18 50 17.303	+00 20 59.01	14.889	12.955	11.843	B0 V	2.12 ^{+0.02} _{-0.03}	3.79 ^{+1.52} _{-1.81}
16	18 50 16.837	+00 21 12.35	13.697	12.006	10.999	B0 V	1.90 ^{+0.01} _{-0.01}	3.51 ^{+1.05} _{-1.43}
17	18 50 17.036	+00 21 46.69	14.326	12.485	11.471	B0 V	2.00 ^{+0.02} _{-0.03}	3.39 ^{+1.35} _{-1.61}
19	18 50 13.554	+00 21 03.23	13.606	11.895	10.981	B0 V	1.84 ^{+0.02} _{-0.03}	2.90 ^{+1.16} _{-1.38}
20	18 50 12.329	+00 20 46.68	14.829	13.25	11.96	B0 V	2.00 ^{+0.02} _{-0.03}	4.23 ^{+1.69} _{-2.01}
21	18 50 10.573	+00 20 25.64	13.727	12.028	11.071	O9.5 V	1.87 ^{+0.01} _{-0.03}	3.32 ^{+0.87} _{-1.14}
s01	18 50 17.623	+00 21 30.65	10.812	8.893	7.839	A2 I	1.89 ^{+0.03} _{-0.01}	3.58 ^{+0.31} _{-0.54}
s03	18 50 15.408	+00 20 58.07	9.232	6.625	5.299	M2 I	1.99 ^{+0.02} _{-0.06}	4.00 ^{+2.82} _{-0.43}
s04	18 50 15.620	+00 21 07.46	9.563	6.984	5.649	M2 I	1.98 ^{+0.02} _{-0.06}	4.72 ^{+3.33} _{-0.51}
s05	18 50 14.117	+00 22 39.56	9.300	6.477	4.938	M1 I	2.25 ^{+0.01} _{-0.06}	2.74 ^{+1.03} _{-0.16}
Fore-/background stars:								
2	18 50 21.558	+00 21 52.31	13.720	12.636	12.054	A0 V	1.10	1.18
10	18 50 14.005	+00 20 06.94	11.281	9.966	9.472	G9–K2 III	0.74	1.32
14	18 50 20.709	+00 21 17.59	10.994	9.638	9.065	G9–K2 III	0.82	1.06
18	18 50 15.788	+00 21 46.06	10.752	9.775	9.391	G0 III	0.61	0.81
22	18 50 10.445	+00 21 03.80	10.499	9.603	9.143	G9–K2 III	0.44	1.31
23	18 50 08.513	+00 22 11.42	11.019	9.528	8.94	G6 III	1.01	0.67
s02	18 50 28.354	+00 21 13.44	11.348	8.935	7.818	K–M I–III

Notes. Equatorial coordinates, near-infrared magnitudes (*J*, *H*, and *K_S*), and spectral classification are given for all stars. For those stars with determined luminosity class are given also the estimated extinction and distance.

but their bluer colours in the CMD might correspond to foreground stars. Spectral classification for this set of stars will clarify the nature and cluster membership for these candidates.

The final group of candidates corresponds to bright and red stars ($K_S < 8$ mag and $(J - K_S) > 3$ mag). These bright objects are red supergiant candidates, separated from the rest of the stars by a ≥ 2 mag gap in K_S . Because these stars are the brightest in the field, they would limit the spectroscopy integration time if they were included in the MOS, causing poor S/N spectra for the dimmer stars. To avoid this, they were observed using long-slit spectroscopy.

The multi-object mask design also considers the positions of the candidates over the field of view. Because the cluster boundaries do not appear to be clearly defined in the LIRIS near-IR images, we included stars not only from the central region of the image but also from the external regions. This would help us to derive information about the membership of stars separated from the central part of the cluster. Besides this, the number and positions of slits in the mask are limited by the spectral overlap in the dispersion axis and the different spectral range observed as a function of the slit position in the field of view. It is necessary to ensure that the spectral range includes the spectral features used for the spectral classification.

4.2. Spectral classification

We based the near-IR spectral classification of the OB stellar types on Hanson et al. (1996) for the *K*-band, and Hanson et al. (1998) for the *H*-band spectra. For later spectral types we used Meyer et al. (1998) and Wallace & Hinkle (1997) for both bands. The characteristic lines for each spectral type were complemented with a visual comparison between our spectra and other spectral catalogues, with *H*- and *K*-band spectra at similar resolutions (Ivanov et al. 2004; Ranade et al. 2004; Ranada et al. 2007; Hanson et al. 2005). For the assigned spectral type we assumed an error of ± 2 subtypes, similar to Hanson et al. (2010), and Negueruela et al. (2010). Table 2 contains the coordinates, near-infrared magnitudes, and spectral types for the spectroscopically observed stars. The positions of these stars in the CMD and pseudo-colour magnitude diagram are presented in Fig. 3. Spectra from masks A and B, and bright stars spectra observed with long-slit are shown in Fig. 4.

One feature that required especial consideration is the spectral ghosts caused by inner reflections in the LIRIS MOS mode. These ghosts appear as emission lines in the image and, if they coincide with the dispersion region defined by a slit, they can mimic a spectral emission line. Because the mask is the origin of

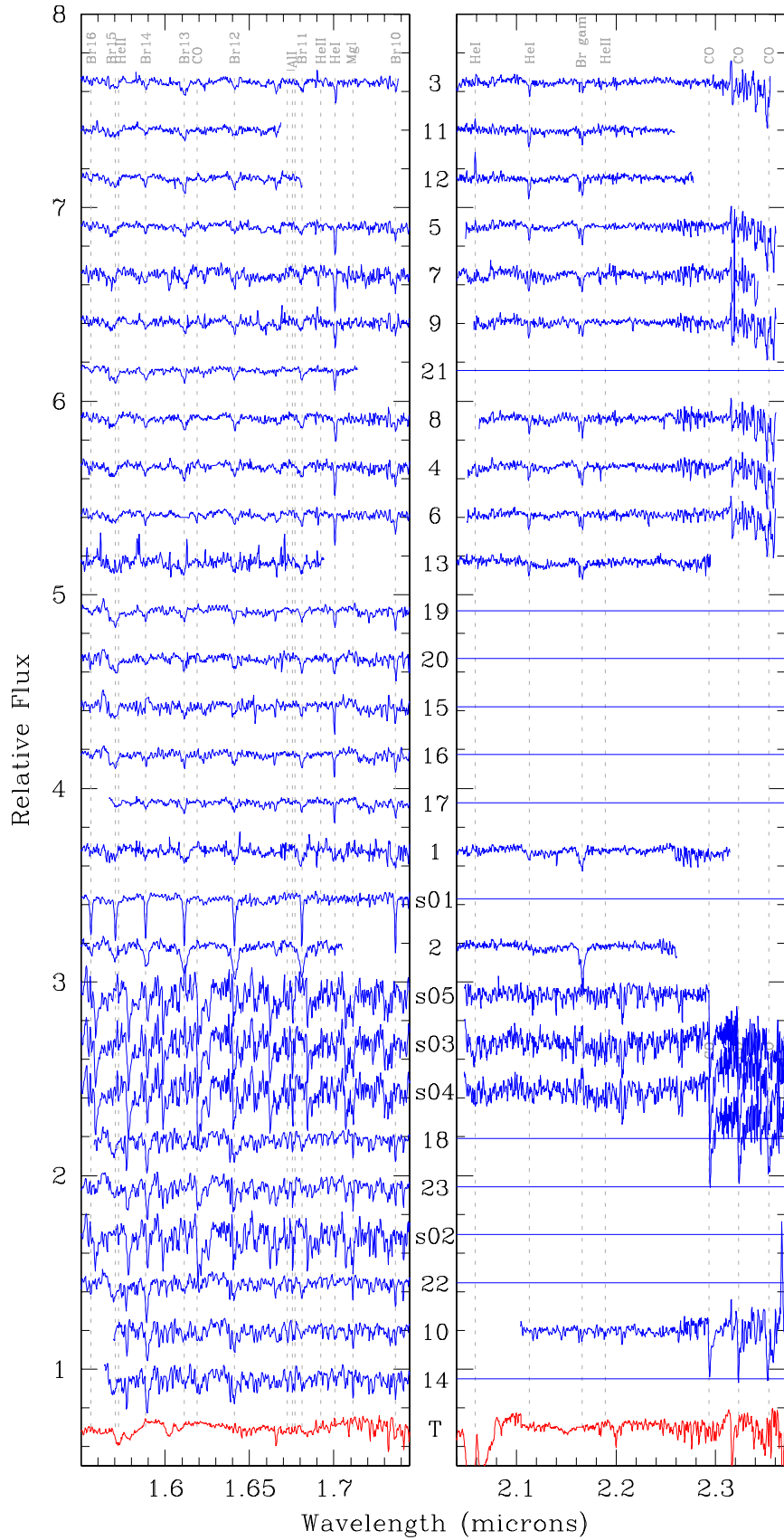


Fig. 4. Individual *H*-band (*left*) and *K*-band spectra (*right*) from mask A, mask B, and long-slit observations. The spectral features used for the spectral classifications are labelled in grey. Spectra are arranged from early- to late-type stars. The bottom red spectrum corresponds to the telluric correction.

ghosts, their positions depend on the slit positions in the mask. After a 180° rotation and shifts in $\delta x = -60$ pixels and $\delta y = -45$ pixels the slit positions coincide with the ghosts positions, making their identification easier.

A visual inspection allowed us to separate the 28 spectra into three groups. The first one is formed by spectra with He I 1.70 μm , He I 2.11 μm , and the Brackett series; this is characteristic of OB-type stars. Spectra of stars with the numbers 1, 3–9, 11–13, 15–17, and 19–21 belong to this group.

The second group is formed by stars with the Brackett series as the only feature in the spectra. Stars number 2 and s01 form this group.

Finally, stars 10, 14, 18, 22, 23, s02, s03, s04, and s05 present Mg I 1.58–1.71 μm lines, Al I 1.67–1.68 μm lines, $^{12}\text{CO } \Delta\nu = 3$ ($^{12}\text{CO } (6, 3)$ at 1.62 μm), and $^{12}\text{CO } \Delta\nu = 2$ bands ($^{12}\text{CO } (2, 0)$ at 2.29, $^{12}\text{CO } (3, 1)$ at 2.32 and $^{12}\text{CO } (4, 2)$ at 2.35 μm), characteristic of late type stars.

The classification of stars from the first group (OB-type) is based on the Brackett series depth, and the presence (and depth) of He I 1.70, 2.06, and 2.11 μm lines. The absence of He II lines indicates spectral types later than O8 for all our stars.

Stars number 3, 11, and 12 are the earliest stars from this group according to their weak Brackett series and the He I 1.70 and 2.11 μm lines. Only H I (4–12), (4–13), and (4–14) are evident, looking similar to O8 V stars (e.g. HD 13268, Hanson et al. 2005), but due to the absence of He II 1.69 μm line the spectral type cannot be earlier than O8.5 V. The depth and shape of He I 1.70 μm and 2.11 μm are similar to O9.5 V stars (for example, HD 37468, Hanson et al. 2005). Because the He I 2.06 μm emission line is not covered into the catalogue spectra, we cannot separate the spectral type for these three stars. Spectral type O9 V is assigned to stars number 3, 11, and 12.

Stars number 5, 7, 8, 9, and 21 display the deepest He I 1.70 μm of the spectral set. Inspection of the sky spectra from their slits discarded the contamination by nebular He I emission, which could have produced an excess of sky correction and thus extra absorption. The depths of this He I line, together with Brackett lines H I (4–11) and H I (4–10), resemble the spectrum of O9.5 V stars (for example, HD 37468, Hanson et al. 2005). For stars number 5, 7, 9, and 21 we assigned spectral type O9.5 V. In the case of star number 8 the Brackett series is slightly deeper, similar to HD 149438 and HD 36822 (B0.2 V stars, Hanson et al. 2005), hence the spectral type for this star is between O9.5 and B0 V.

For stars number 13, 19, and 20, the Brackett series looks deeper than for stars number 11 and 12. The depths of He I 2.11 μm and H I (4–7) are similar to spectral B0 V types (for example, HD 6165 Wallace & Hinkle 1997). Spectral type B0 V was therefore adopted for these stars.

Spectra from stars number 1, 4, and 6 show clear Brackett series until H I (4–15). The H I (4–7) line is deeper than He I 2.11 μm , indicating dwarf luminosity class (e.g. B1 V star HD 191639 and B1 V HD 31726; Hanson et al. 1996). The similarity of the Brackett series and He I lines to the mentioned stars implies a B1 V spectral type for star number 1. For stars number 4 and 6, the depth of He I 1.70 μm and the similar H I (4–10) line to stars number 13, 19, and 20 imply an earlier spectral type (B0 V).

Finally, three stars from this group (stars number 15, 16, and 17) exhibit narrow He I 1.70 μm that would indicate luminosity class III. Unfortunately, the lack of *K*-band spectra – and the associated He I 2.11 μm line – does not allow a clear differentiation between luminosity classes V and III. Nonetheless, the individual distance estimates for these three stars under the

assumption of a luminosity class III are higher (5.80, 5.16 and 6.12 kpc for stars number 15–17) than the calculated for luminosity class V, which agrees with the rest of the stars. Because for both luminosity classes the estimated individual extinctions are the same, we consider it to be highly unlikely that these three stars belong to another cluster located at ~ 5.5 kpc, in the same line of sight as Masgomas-1, without additional extinction. These arguments, together with the central position of the stars in the cluster’s field of view favour luminosity class V for these three stars. The clear Brackett series between H I (4–15) and H I (4–10) implies a spectral type B0 V.

The spectrum of star number 2 presents neither He I nor He II lines. The H I (4–7) line indicates a star later than B8 V (HD 169990, Hanson et al. 2005), and fits an A0 V star (for example, HR 5793, Meyer et al. 1998). Later spectral types show a deeper line. The Brackett series fits an A0 V star from H I (4–18) to H I (4–11) (e.g. HD 122945, previously observed with LIRIS, and HR 7001, Meyer et al. 1998). The blue colour for this star compared with the other observed stars and the A0 V spectral type indicate that star number 2 is a foreground star.

As mentioned previously, stars number 10, 14, 18, 22, and 23 show lines characteristic of late-type stars (e.g. Mg I 1.58–1.71 μm , Al I 1.67–1.68 μm , and $^{12}\text{CO } \Delta\nu = 3$ bands). The $^{12}\text{CO } \Delta\nu = 2$ bands of star number 10 are similar in depth to an early K III star. The Mg I 1.58–1.71–2.28 μm and $^{12}\text{CO } \Delta\nu = 3$ bands are characteristic of G9–K2 III stars (e.g. HR 7328, HR 5340 or HR 7806, Meyer et al. 1998). Star number 10 is classified as a foreground G9–K2 III source.

The *H*-band spectra of stars number 14 and 22 are similar to the spectrum of star number 10. A better spectral classification than obtained for star number 10 without the *K*-band spectra is not possible. Hence, for stars number 14 and 22 we assigned the same spectral type as for star number 10.

The spectra of stars number 18 and 23 look similar to the spectrum of star number 10 but with minor differences. Star number 18 shows a smaller $^{12}\text{CO } \Delta\nu = 2$ band and Mg I 1.58–1.71 μm lines. The *H*-band spectrum is similar to that of a G0 III star (for example, HR 4883, Meyer et al. 1998), which is the spectral type assigned to star number 18. The spectrum of star number 23 has deeper Mg I 1.58–1.71 μm lines than star number 18. Because its spectrum looks similar to that of star HR 4716 (G6 III star, Meyer et al. 1998), we assigned a G6 III spectral type to this star.

Long-slit spectra for the five bright stars (s01, s02, s03, s04, and s05) show the characteristics of giant/supergiant stars. For example, the spectrum of s01 is dominated by a narrow Brackett series, typical of luminosity class I (Meyer et al. 1998). The absence of He I 1.70 μm discounts a late B-type star, and the depth of the hydrogen lines is similar to that for an A I star. The depths of the Ne II line at 1.77 μm and the H I (4–10), (4–11), (4–12), and (4–13) lines indicate an A2 spectral type for s01 (like star HR 7924, Meyer et al. 1998).

The spectra of s02, s03, s04 and s05 show strong $^{12}\text{CO } \Delta\nu = 3$ and $^{12}\text{CO } \Delta\nu = 2$ (for s03, s04 and s05) bands associated with late K–M giant and supergiant stars. For s03, s04 and s05, the equivalent width (*EW*) of $^{12}\text{CO } (2, 0)$ corresponds to luminosity class I. For them we measured $EW_{s03} = 31.37 \text{ \AA}$, $EW_{s04} = 31.47 \text{ \AA}$ and $EW_{s05} = 27.89 \text{ \AA}$, in the region between 2.294 and 2.304 μm . For early M-stars, these values lie in the supergiant zone in the relation given by Davies et al. (2007), but differences in the spectral lines and molecular band depth for the early M-star subclasses are hard to find at our spectral resolution. For s03 and s04 the depth of the $^{12}\text{CO } \Delta\nu = 3$ bands

is more similar to an M2 (e.g. HD 14479; Meyer et al. 1998) than to an M1 star (e.g. HD 339034; Meyer et al. 1998) or to an M4-5 source (e.g. HR 7009; Meyer et al. 1998). The depth of s05 is indicative of an earlier spectral subtype (M1 I).

For star s02 the luminosity class is not straightforward to define because of the lack of K -band spectroscopy. The softer continuum (compared with s03 and s04) and the distance from the cluster centre (~ 3.2 arcmin) support a fore-/background giant star classification for s02, but we cannot clearly decide between luminosity classes III or I for this object.

4.3. Proper motion

To measure OB-type and supergiant stars proper motions, we followed a similar procedure as described by Peña Ramírez et al. (2011). We used the 2MASS image as the first epoch and the LIRIS image as the second epoch, with a time baseline of 10.88 years. The spatial transformation between both epochs image coordinate systems was performed with 370 resolved stars well distributed over the whole LIRIS image, with $K_S < 14$. For stellar positions we used the centroids given in the 2MASS catalogue and the coordinates derived from LIRIS photometry. Objects classified as early-type and supergiants were excluded from the set of calibration stars to avoid the inclusion of cluster stars in the transformation calculation. The dispersion of the transformation is 0.25 pix for x and 0.30 pix for y . Because these values are higher than the errors in the object's centroid determination, we adopted them as mean proper motion errors.

After obtaining the parameters for the transformation, we calculated the pixel shifts for the four supergiants (stars s01, s03, s04, and s05) and the OB-type stars (stars number 3–6, 8, 11–13, 17, and 19), OB-type stars without 2MASS photometry were not included in the proper motion determination. To finally convert the pixel shifts into proper motions, we divided by the time baseline between both epochs (i.e. 10.88 years), and multiplied by the pixel scale of LIRIS image. The obtained proper motions are presented in Fig. 5.

In Fig. 5 we present in grey dots the proper motions for the references stars. This group of stars could include unidentified cluster members, foreground and background stars. Proper motions for the identified cluster stars and six foreground stars are labelled with the same identification numbers as used in Sect. 4.2. In the figure we can see that most of the LIRIS field of view stars are within the 2σ uncertainty ellipse. No proper motion difference between cluster and fore-/background stars can be detected with our resolution.

5. Discussion

5.1. Distance estimate

Using the estimated spectral types, we derived individual distances for the cluster stars. Assuming the absolute visual magnitudes from Cox (2000), intrinsic infrared colours from Tokunaga (2000), and the Rieke et al. (1989) extinction law with $R = 3.09$ (Rieke & Lebofsky 1985), the extinction for the K_S band may be expressed as

$$A_{K_S} = \frac{E_{J-K_S}}{1.514} = \frac{E_{H-K_S}}{0.561}. \quad (1)$$

Extinction ranges from 1.10 to 2.33 mag for A_{K_S} , or A_V between 10.15 and 21.49 mag. In Table 2 we present the values of extinction and individual distances for the OB-type stars and the supergiant stars. The mean of these individual distances

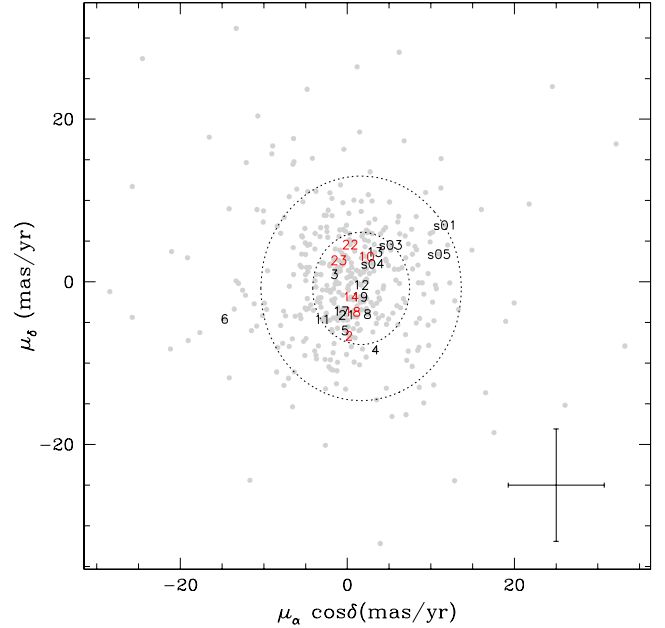


Fig. 5. Proper motions for OB-type and supergiant stars of Masgomas-1. Grey circles indicate the proper motions for stars without spectral follow-up (unidentified cluster members, foreground and background stars), and black numbers show the proper motion for cluster massive stars, classified spectroscopically. Red numbers indicate the proper motion for foreground stars, derived from the spectroscopic observations. In the bottom right corner of the figure we show the mean error for the proper motions ($\Delta(\mu_\alpha \cos \delta) = 5.75$ and $\Delta(\mu_\delta) = 6.91$). Ellipses represent 1σ and 2σ proper motion uncertainties.

is $3.53^{+1.55}_{-1.40}$ kpc, our estimate for the distance to Masgomas-1. For comparison we estimated the individual distances using the Indebetouw et al. (2005) extinction law, obtaining lower values for them. The mean distance estimated using this extinction law is $3.50^{+1.55}_{-1.40}$ kpc, which is consistent with the estimate obtained using the Rieke et al. (1989) extinction law to within the errors. Late-type giant stars were excluded from the distance estimate because their individual distance estimates imply that they are not part of the cluster and probably belong to the disc population.

Even if Masgomas-1 is located in the same direction as the base of the Scutum-Centaurus Arm our estimate positions the cluster closer than the red supergiant clusters (RSGC). Distances for RSGC 1, 2, 3 and 4 (6.60, 5.83, 6, and 6.6 kpc respectively; Clark et al. 2009a; Negueruela et al. 2010) indicate that they belong to the intersection of the tip of the Galactic bar and the base of the Scutum-Centaurus Arm. Our estimate of 3.53 kpc and the galactic coordinates for Masgomas-1 place it in the Scutum-Centaurus arm itself but without any evidence relating it with the star-forming region located in the intersection between the end of the Galactic bar and the base of the Scutum-Centaurus arm.

5.2. Mass and age estimate

We estimated the total mass of Masgomas-1 by integrating the initial mass functions, fitted to the cluster mass function. This was performed separately for a Salpeter and a Kroupa initial mass function (IMF). The Salpeter IMF (Salpeter 1955) was fitted to the cluster's massive population: the O-type dwarf and the supergiant stars. We used this IMF for the first estimate to compare it with the values given by RSGC 3 and Cl Alicante 8.

The O-type dwarf population is formed by eight stars with spectral type between O9–O9.5 V and mass between 15 and 18 M_{\odot} (Martins et al. 2005). The integration of a Salpeter function indicates that a 11 000 M_{\odot} initial mass is expected for the cluster to have a population of eight O-type dwarfs. This number could be underestimated, because we only included those stars in the population that were observed spectroscopically and with the subsequent spectral classification.

For the supergiant population, formed by stars s01, s03, s04 and s05, the same method indicates that a cluster of 8000–9000 M_{\odot} is required to host a population of four supergiant stars, with initial mass of $\sim 20 M_{\odot}$, determined using evolutionary tracks from Marigo et al. (2008).

In both populations we integrated the Salpeter IMF from $\log(M) = -1.0$ dex to 1.3 dex. The first limit corresponds to the stellar lower limit ($\sim 0.1 M_{\odot}$) and the second one corresponds to the most massive star detected in our work for Masgomas-1. Our estimate for the total mass of Masgomas-1 is between 8000 and 11 000 M_{\odot} .

This estimate agrees with the initial total mass obtained for other clusters with a red supergiant population. For RSGC 3, Clark et al. (2009a) estimated a total mass of $(2-4) \times 10^4 M_{\odot}$, and for Cl Alicante 8 (Negueruela et al. 2010) the total initial mass is estimated to be $2 \times 10^4 M_{\odot}$. Both clusters contains eight supergiants, therefore a higher initial total mass is expected. Our total mass estimate also agrees with the simulations presented by Clark et al. (2009b), where three red supergiants are expected for clusters with a total mass over $10^4 M_{\odot}$.

The second estimate of the cluster total mass was obtained using the cluster initial mass function, ranging from $\sim 3 M_{\odot}$ to $\sim 30 M_{\odot}$. The mass function was derived from the luminosity function, corrected for the field stellar contribution using a control field. We fitted a Kroupa IMF (Kroupa 2001) to the mass histogram and integrated within the same limits used for our first estimate (i.e. from $\log(M) = -1.0$ dex to 1.3 dex). Because we had no LIRIS photometry for a control field, we used UKIDSS³ (for $K > 9.3$) and 2MASS (for $K_S < 9.3$) photometry for both Masgomas-1 and control fields. The circular area for the control field is centred on $\alpha_{2000} = 18^{\text{h}}49^{\text{m}}47^{\text{s}}$, $\delta_{2000} = +00^{\circ}13'36''$, and it has a radius of 3'. The same radius was used to obtain the photometry for the Masgomas-1 field.

To correct the difference between both photometric systems, we used the transformation equations given by Carpenter (2001). For the UKIDSS photometry we used data for $J < 18.1$, $H < 16.8$, and $K < 16.1$, to ensure completeness close to 1.0 for the data. These limiting magnitudes were determined from the star count histograms for each filter, the magnitude where the star counts start to decrease was defined as the limiting magnitude.

To obtain the luminosity and mass functions for both fields, we followed the same procedure as described by Ramírez Alegría et al. (2011). First, we projected every star following the reddening vector to the dwarf star sequence, located at our estimated distance, and defined by the magnitudes and colours of Cox (2000). This sequence is expressed analytically by two lines, one from O9 V to A0 V and the second from A0 V to G2 V. The cut in G2 V arises from the selected limiting magnitude for the UKIDSS photometry.

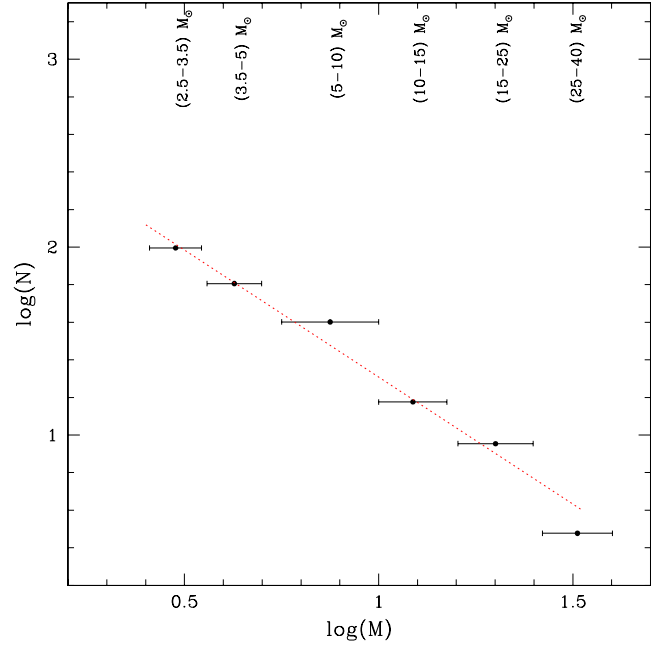


Fig. 6. Mass function for Masgomas-1. The points indicate the central position of the mass range indicated above. The segmented red line shows the Kroupa IMF fitted to the data.

Once the stars in the Masgomas-1 and the control field CMDs were projected following the reddening vector to the line-fitted main sequence, we derived the luminosity functions. We converted the K magnitude to stellar mass using the values given by Cox (2000), obtaining the mass functions. For magnitudes that were in between values from the catalogue, we interpolated between the two closest values.

After subtracting both mass functions (i.e. Masgomas-1 field minus control field), we obtained the cluster initial mass function (shown in Fig. 6). We fitted a multiple segment Kroupa IMF⁴, and integrated it in the range 0.10 to 20 M_{\odot} , obtaining a total mass for Masgomas-1 of $(1.94 \pm 0.28) \times 10^4 M_{\odot}$. This value is higher than estimated by fitting a Salpeter IMF only to the massive cluster population, but it considers a wider range of mass for the cluster population, and confirms the massive nature of the cluster.

For the age estimate we derived information based on the earliest main-sequence star or the presence of red supergiant stars. In the first case, the O9 V star indicates an age upper limit of 10 Myr, which is the time spent by an O9 star in the main sequence, depending on the initial rotational velocity (Brott et al. 2011).

On the other hand, the M-type red supergiants position in the CMD could be described with an isochrone, but caution has to be taken because the supergiant’s intrinsic colours are not well constrained. As mentioned by Negueruela et al. (2010), the extinction correction for supergiants can be made incorrectly due to colour terms or the structure of their atmospheres. Because of that, we prefer not to estimate the cluster age by fitting an isochrone to the predicted intrinsic magnitudes and colours of the red supergiants.

³ The UKIDSS project is defined in Lawrence et al. (2007). UKIDSS uses the UKIRT Wide Field Camera (WFCAM; Casali et al. 2007). The photometric system is described in Hewett et al. (2006), and the calibration is described in Hodgkin et al. (2009). The pipeline processing and science archive are described in Hambly et al. (2008).

⁴ As mentioned by Clark et al. (2009b), an estimate of the total mass cluster by integrating a Salpeter IMF overestimates the low-mass stars contribution, resulting in a difference of $\sim 30\%$ between the two total mass estimates.

According to Davies et al. (2007), red supergiants are expected in massive clusters after ~ 6 Myr, which is a lower limit that is compatible with the upper limit set by the O9 V star. In their Fig. 2, we can see that a $2 \times 10^4 M_{\odot}$ cluster of ~ 6.5 Myr should contain 3 or 4 red supergiants. For less massive clusters the needed age for that number of red supergiants would be higher, but hardly higher than the upper limit set by the earliest main sequence star in Masgomas-1. For example Fig. 3 from Clark et al. (2009b) shows that a $10^4 M_{\odot}$ cluster would present three red supergiants after ~ 10 Myr, still an upper limit consistent with the one set by the presence of an O9 V cluster star.

With these arguments, we estimate an age for Masgomas-1 between 8 to 10 Myr.

6. Conclusions

As part of our systematic search and physical characterization of massive stellar clusters, we completed a spectrophotometric study of Masgomas-1, the first cluster discovered by our MASGOMAS project. This study was completed using photometric and spectroscopic LIRIS data obtained at the WHT.

With the new near-infrared data and the reddening-free Q_{IR} parameter, we selected 23 OB-type candidates for H and K spectroscopy. Five bright red stars from the Masgomas-1 field of view were selected as red supergiant candidates and for H and K spectroscopy. These 28 stars were spectrally classified and individual spectrophotometric distances were estimated for the OB-type and supergiant stars. The individual distances and the associated individual extinctions are consistent with a common distance for all objects. For all supergiants (one yellow and three red) and ten of the OB-type stars, we measured proper motions. The resolution of the proper motion measures did not allow us to find differences between the individual distances of these stars.

Using the individual distance estimate, we obtained a distance to Masgomas-1 of $3.53^{+1.55}_{-1.40}$ kpc, placing Masgomas-1 in the Scutum-Centaurus arm, but far from the arm base.

For the cluster total mass we obtained a lower limit, adjusting a Salpeter function to the most massive stars in our work. Integrating this function between 20 and $0.1 M_{\odot}$, we obtained a total mass of $(0.8-1.1) \times 10^4 M_{\odot}$. We repeated this procedure using the initial cluster mass function fitted with a Kroupa function. Integration of this function in the same mass range confirms the massive nature of Masgomas-1 (i.e. over $10^4 M_{\odot}$), and gives a higher estimate for the cluster's total mass: $(1.94 \pm 0.28) \times 10^4 M_{\odot}$.

The cluster age could be limited in two ways: an upper limit given by the earliest star in the cluster's main sequence of 10 Myr, and a lower limit given by the presence of the M-type supergiants, estimated between 6.5 and 10 Myr. The latest limit varies according to the total initial mass of the cluster, which remains compatible with the upper limit of 10 Myr set by the presence of the O9 V star.

Acknowledgements. S.R.A. was supported by the investigation project Massive Stars in Galactic Obscured Massive Clusters. Part of this work was supported by the Science and Technology Ministry of the Kingdom of Spain

(grants AYA2008-06166-C03-01, and AYA2010-21697-C05-04), the Gobierno de Canarias (PID2010119), and the Fundación Agencia Aragonesa para la Investigación y Desarrollo (ARAID). S.R.A., A.H., and A.M-F. are members of the Consolider-Ingenio 2010 Programme (CSD2006-00070). The *William Herschel* Telescope is operated on the island of La Palma by the Isaac Newton Group in the Spanish Observatorio del Roque de los Muchachos of the Instituto de Astrofísica de Canarias. This publication makes use of data products from the Two Micron All Sky Survey, which is a joint project of the University of Massachusetts and the Infrared Processing and Analysis Center/California Institute of Technology, funded by the National Aeronautics and Space Administration and the National Science Foundation.

References

- Benjamin, R. A., Churchwell, E., Babler, B. L., et al. 2003, *PASP*, 115, 953
 Brott, I., de Mink, S. E., Cantiello, M., et al. 2011, *A&A*, 530, A115
 Carpenter, J. M. 2001, *AJ*, 121, 2851
 Casali, M., Adamson, A., Alves de Oliveira, C., et al. 2007, *A&A*, 467, 777
 Clark, J. S., Negueruela, I., Davies, B., et al. 2009a, *A&A*, 498, 109
 Clark, J. S., Davies, B., Najarro, F., et al. 2009b, *A&A*, 504, 429
 Comerón, F., & Pasquali, A. 2005, *A&A*, 430, 541
 Cox, A. N. 2000, *Allen's Astrophysical Quantities*, 4th edn. (New York: Springer)
 Davies, B., Figer, D. F., Kudritzki, R.-P., et al. 2007, *ApJ*, 671, 781
 Davies, B., Figer, D. F., Law, C. J., et al. 2008, *ApJ*, 676, 1016
 Eikenberry, S., Elston, R., Raines, S. N., et al. 2006, in *Ground-based and Airborne Instrumentation for Astronomy*, ed. I. S. McLean, & M. Ian (Washington: SPIE), Proc. SPIE, 6269, 626917
 Figer, D. F., MacKenty, J. W., Robberto, M., et al. 2006, *ApJ*, 643, 1166
 Hambly, N. C., Collins, R. S., Cross, N. J. G., et al. 2008, *MNRAS*, 384, 637
 Hanson, M. M., & Popescu, B. 2008, in *Massive Stars as Cosmic Engines*, ed. F. Bresolin, P. A. Crowther, & J. Puls (Cambridge: Cambridge Univ. Press), IAU Symp., 250, 307
 Hanson, M. M., Conti, P. S., & Rieke, M. J. 1996, *ApJS*, 107, 281
 Hanson, M. M., Rieke, G. H., & Luhman, K. L. 1998, *AJ*, 116, 1915
 Hanson, M. M., Kudritzki, R., Kenworthy, M. A., Puls, J., & Tokunaga, A. T. 2005, *ApJS*, 161, 154
 Hanson, M. M., Kurtev, R., Borissova, J., et al. 2010, *A&A*, 516, A35
 Hewett, P. C., Warren, S. J., Leggett, S. K., & Hodgkin, S. T. 2006, *MNRAS*, 367, 454
 Hodgkin, S. T., Irwin, M. J., Hewett, P. C., & Warren, S. J. 2009, *MNRAS*, 394, 675
 Inebetouw, R., Mathis, J. S., Babler, B. L., et al. 2005, *ApJ*, 619, 931
 Ivanov, V. D., Rieke, M. J., Engelbracht, C. W., et al. 2004, *ApJS*, 151, 387
 Kroupa, P. 2001, *MNRAS*, 322, 231
 Lawrence, A., Warren, S. J., Almaini, O., et al. 2007, *MNRAS*, 379, 1599
 Marigo, P., Girardi, L., Bressan, A., et al. 2008, *A&A*, 482, 883
 Marín-Franch, A., Herrero, A., Lenorzer, A., et al. 2009, *A&A*, 502, 559
 Martins, F., Schaerer, D., & Hillier, D. J. 2005, *A&A*, 436, 1049
 Meyer, M. R., Edwards, S., Hinkle, K. H., & Strom, S. E. 1998, *ApJ*, 508, 397
 Negueruela, I., & Schurch, M. P. E. 2007, *A&A*, 461, 631
 Negueruela, I., González-Fernández, C., Marco, A., Clark, J. S., & Martínez-Núñez, S. 2010, *A&A*, 513, A74
 Peña Ramírez, K., Zapatero Osorio, M. R., Béjar, V. J. S., Rebolo, R., & Bihain, G. 2011, *A&A*, 532, A42
 Ramírez Alegría, S., Herrero, A., Marín-Franch, A., et al. 2011, *A&A*, 535, A8
 Ranade, A., Gupta, R., Ashok, N. M., & Singh, H. P. 2004, *Bull. Astron. Soc. India*, 32, 311
 Ranada, A. C., Singh, H. P., Gupta, R., & Ashok, N. M. 2007, *Bull. Astron. Soc. India*, 35, 87
 Rieke, G. H., & Lebofsky, M. J. 1985, *ApJ*, 288, 618
 Rieke, G. H., Rieke, M. J., & Paul, A. E. 1989, *ApJ*, 336, 752
 Salpeter, E. E. 1955, *ApJ*, 121, 161
 Skrutskie, M. F., Cutri, R. M., Stiening, R., et al. 2006, *AJ*, 131, 1163
 Stetson, P. B. 1994, *PASP*, 106, 250
 Tokunaga, A. T. 2000, *Infrared Astronomy* (Springer), 143
 Vacca, W. D., Cushing, M. C., & Rayner, J. T. 2003, *PASP*, 115, 389
 Wallace, L., & Hinkle, K. 1997, *ApJS*, 111, 445